NOTES AND CORRESPONDENCE

The Effects of Dissipative Heating on Hurricane Intensity

DA-LIN ZHANG AND ERIC ALTSHULER

Department of Meteorology, University of Maryland, College Park, Maryland

14 May 1998 and 6 October 1998

ABSTRACT

The effects of dissipative heating on hurricane intensity are examined using a 72-h explicit simulation of Hurricane Andrew (1992) with a state-of-the-art, three-dimensional, nonhydrostatic mesoscale (cloud resolving) model (i.e., MM5). It is found that the inclusion of dissipative heating increases the central pressure deficit of the storm by 5–7 hPa and its maximum surface wind by about 10% prior to landfall. It is shown that dissipative heating tends to warm the surface layer, causing a decrease (increase) in sensible heat flux at the sea surface (the top of the surface layer) that acts to cool the surface layer, although the net (sensible plus dissipative) heating rates are still 30%–40% greater than the sensible heating rates in the control simulation. Finally, the potential effects of energy transfer into the ocean, sea surface temperature changes within the inner core, and evaporation of sea spray, interacting with dissipative heating, on hurricane intensity are discussed.

1. Introduction

Recently, Bister and Emanuel (1998) pointed out that the effects of dissipative heating have traditionally been neglected in numerical hurricane models and in theoretical estimates of the maximum potential intensity of hurricanes. They showed, using two independent theoretical derivations, that the inclusion of dissipative heating in the boundary layer increased maximum wind speeds by approximately 20%. They also presented results from two idealized numerical simulations, one using an axisymmetric three-layer balance model (Emanuel 1995) and the other an axisymmetric, nonhydrostatic model that explicitly resolves convective clouds (Rotunno and Emanuel 1987). For the balance model, they reported an increase in maximum wind speeds of approximately 30% and a 60% increase in the central pressure deficit relative to the environment, when compared to the corresponding simulation without dissipative heating. For the nonhydrostatic model, the wind speed increase was approximately 25% when the maximum speed reaches 90 m s^{-1}, while the central pressure deficit increased by roughly 40%.

The purpose of this note is to examine the effects of dissipative heating on hurricane intensity through a high-resolution, real-data, explicit simulation of Hurricane Andrew (1992) with a state-of-the-art three-dimensional, nonhydrostatic cloud-resolving model. Specifically, Liu et al. (1997) performed a 72-h, explicit simulation of the storm using the Pennsylvania State University–National Center for Atmospheric Research (PSU–NCAR) mesoscale model (i.e., MM5). This simulation resulted in a generally satisfactory reproduction of Andrew's track, central pressure, maximum surface winds, and inner-core structures. In this study, we repeat this simulation with the effects of dissipative heating included (expt DIS) and compare some of the results with those from the control simulation (expt CTL).

The next section provides a brief overview of the MM5 model and the construction of the initial conditions. Section 3 shows the formulation of dissipative heating in the thermodynamic energy equation. Section 4 presents selected results from the dissipative heating simulation and compares them with the corresponding results from the control simulation. A summary and discussions on the potential effects of the atmosphere–ocean coupling and evaporation of sea spray are given in the final section.

2. Model description and initial conditions

The PSU–NCAR model (i.e., MM5) used for this study is a nonhydrostatic, two-way interactive, movable, triply nested grid mesoscale model; see Dudhia (1993) and Grell et al. (1995) for a detailed description. The designs of the multiple meshes and model configuration are identical to those used by Liu et al. (1997). That is, the model integration employs three nested grid lengths

Corresponding author address: Dr. Da-Lin Zhang, Department of Meteorology, University of Maryland, College Park, MD 20742-2425.
E-mail: dalin@atmos.umd.edu

of 54, 18, and 6 km, with 23 σ-coordinate layers in the vertical.

The Betts–Miller (1986) cumulus parameterization scheme is used to remove any conditionally unstable atmospheric columns over the 54- and 18-km grid mesh domains. For the 6-km mesh domain, the water cycle is explicitly treated using the Tao–Simpson (1993) cloud microphysics scheme (i.e., cloud resolving), which contains prognostic equations for cloud water, ice, rainwater, snow, and graupel. This explicit scheme is also used in coupling with the Betts–Miller cumulus scheme over the 54- and 18-km mesh domains (see Zhang et al. 1988 for pertinent discussion). Other model physics include a modified version of the Blackadar (1979) planetary boundary layer (PBL) parameterization (Zhang and Anthes 1982) and a cloud–radiation interaction scheme (Dudhia 1989; Grell et al. 1995). The sea surface temperature (SST) is held constant in time during the integration, and the surface friction over ocean is calculated using a roughness length that is dependent on the surface wind speed (Delsol et al. 1971). The land surface temperature is predicted using a surface energy budget equation, in which the effects of short- and longwave radiation and cloud radiation are included.

The model is initialized at 1200 UTC 21 August 1992 with the National Centers for Environmental Prediction 2.5° × 2.5° (latitude–longitude) resolution analysis, which is then enhanced by rawinsonde and surface observations and the U.S. Navy's SST field. As shown by Kurihara et al. (1993, 1995), among others, a proper representation of the scale and intensity of the initial vortex, which is lacking in the analysis, is important for a successful forecast of the track and intensity of a hurricane. Liu et al. (1997) constructed a synthetic vortex by running the model for 48 h from the above initial time, extracting the resulting vortex, and merging it into the original initial conditions at the location consistent with the best track analysis at the initial time. The reader is referred to Liu et al. (1997) for a more complete discussion.

In the present study, the control simulation was obtained by duplicating the simulation of Liu et al. (1997), using a somewhat more recent version of the MM5 and running it on a DEC Alpha workstation instead of a CRAY Y-MP. Although there were some small differences in the simulated track and intensity of Andrew from the results of Liu et al. (1997), the overall agreement with their results was quite good.

3. Parameterization of dissipative heating

It is well known that the frictional dissipation of kinetic energy occurs at molecular scales, and it is ultimately converted into thermal energy (i.e., heat). In order to obtain an expression for the rate of production of thermal energy by frictional dissipation, we first form an equation for the kinetic energy tendency by taking the dot product of the horizontal momentum equation:

$$\frac{\partial K}{\partial t} = -\mathbf{V}\cdot\nabla K - w\frac{\partial K}{\partial z} - \mathbf{V}\cdot\frac{\nabla p}{\rho} + \mathbf{V}\cdot\mathbf{F}, \quad (1)$$

where $K = \mathbf{V}\cdot\mathbf{V}/2$, $\mathbf{V}$ is the horizontal wind velocity, $\mathbf{F}$ is the momentum tendency due to frictional effects, and the other symbols assume their usual meteorological meaning. In the free atmosphere of a numerical model, $\mathbf{F}$ represents the influence of (subgrid scale) Reynolds's stress (or momentum fluxes) on the resolvable-scale flow and it is parameterized as horizontal and vertical numerical diffusions that are mainly used to ensure computational stability. They are normally one to two orders of magnitude smaller than advection terms in the horizontal momentum equation. Although the vertical momentum fluxes are large in the PBL, only momentum transfer (i.e., a diffusive process) between layers occurs. However, *at the bottom boundary,* large kinetic energy tends to be lost and it should eventually be converted to heat at molecular scales; so it is called dissipative heating. It is this portion of kinetic energy that has been neglected by current numerical models. To include the dissipative heating, let us begin with the surface-layer averaged momentum ($\mathbf{V_a}$) tendency due to friction that can be represented by the vertical gradient of stress τ, that is,

$$\left.\frac{\partial \mathbf{V}_a}{\partial t}\right|_{\text{Fric}} = \frac{1}{\rho}\frac{\partial \tau}{\partial z} = \frac{1}{\rho}\frac{\tau_1 - \tau_g}{z_1}, \quad (2)$$

where subscripts 1 and g denote the top of the surface layer and the ground, respectively; subscript a denotes the lowest half-σ level (i.e., at the middle of the surface layer) as a result of using the vertically staggered grid; and z_1 (=80 m in the present case) is the thickness of the surface layer. The ground stress τ_g is calculated from

$$\tau_g = \rho u^{*2}, \quad (3)$$

where u^* is the friction velocity and it is a function of the surface wind speed, roughness, and stability (see Zhang and Anthes 1982). The rate of change of kinetic energy in the surface layer due to the PBL processes can be written as

$$\left.\frac{\partial K}{\partial t}\right|_{\text{Fric}} = \frac{\mathbf{V}_a}{\rho}\cdot\frac{\tau_1 - \tau_g}{z_1}. \quad (4)$$

The sink of kinetic energy at the bottom boundary due to frictional dissipation can then be expressed as

$$\left.\frac{\partial K}{\partial t}\right|_{\text{Dis}} = -\frac{|\mathbf{V_a}|}{\rho}\frac{\tau_g}{z_1}. \quad (5)$$

In order for total energy to be conserved, the kinetic energy lost due to frictional dissipation must be returned to the system as thermal energy. Thus, the term on the right-hand side of Eq. (5) has to be incorporated into the thermodynamic energy equation, that is,

$$\left.\frac{\partial T}{\partial t}\right|_{\text{Dis}} = \frac{|\mathbf{V}_a|\tau_g}{\rho c_{\text{pm}} z_1}, \quad (6)$$

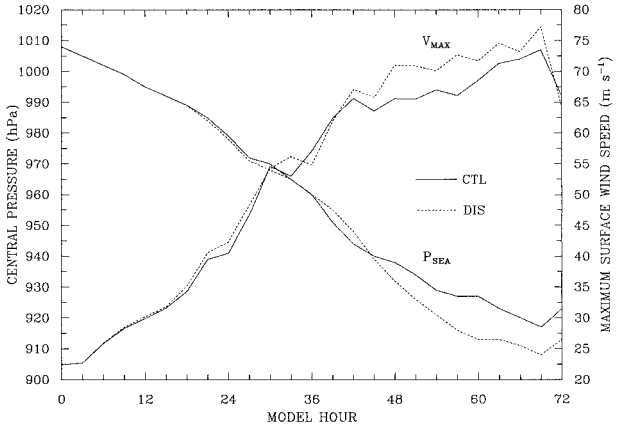

FIG. 1. Time series (3 hourly) of the minimum central sea level pressure (P_{SEA}, hPa) and maximum wind speed (V_{MAX}, m s^{-1}) in the model surface layer ($\sigma = 0.995$) from expts CTL (solid) and DIS (dashed). Landfall occurs at 68 h into the integration.

where c_{pm} is the specific heat of moist air at constant pressure. Clearly, the dissipative heating in the surface layer depends on the thickness of the surface layer, the friction velocity, and the surface wind speed. The stronger the surface winds, the more rapid is the increase in the dissipative heating since the latter is approximately proportional to a cubic power of the surface wind speed (i.e., $|\mathbf{V_a}|^3$). It follows that the magnitude of dissipative heating is much greater over ocean than over land.

It is generally believed that the rate at which atmospheric kinetic energy is transferred to the ocean by the wind stress is between one and two orders of magnitude smaller than that given by Eq. (5) (Richman and Garrett 1977; Hellerman and Rosenstein 1983; J. Carton 1998, personal communication). Thus, we may ignore this process and convert the entire kinetic energy sink at the bottom boundary to dissipative heating as given in Eq. (6). We have also ignored (interior) dissipative heating above the surface layer as done in most PBL parameterization schemes, since it decreases rapidly with height as the size of turbulent eddies increases (Stull 1988; Bister and Emanuel 1998).

For a more detailed description of the prognosis of the horizontal momentum and temperature in the surface layer, the vertical model configuration, the friction velocity, surface fluxes, and other surface-layer variables, the reader is referred to Zhang and Anthes (1982) and Grell et al. (1995).

4. Results

In this section, we present the time series and horizontal distributions of several surface-layer quantities from the 72-h explicit integration of Hurricane Andrew (1992) in an attempt to better understand the processes by which dissipative heating contributes to intensity changes in a hurricane. Figure 1 shows the 3-hourly time series of central pressure and maximum surface (i.e., the lowest half-σ level, $\sigma = 0.995$, a height of approximately 40 m above the sea level) wind speed for the control (CTL) and dissipation (DIS) runs. It is apparent that the inclusion of dissipative heating has resulted in a more intense storm. Specifically, the maximum surface wind speed in experiment DIS, after it reaches 70 m s^{-1} at 48 h and before landfall at 68 h, is about 10% greater than that in experiment CTL, and the increase in central pressure deficit relative to the environment (taken to be 1016 hPa) is roughly 15%. If the storm were allowed to continue its evolution in the same oceanic environment, we may expect it to keep deepening and the differences between the two runs to increase to the extent as shown by Bister and Emanuel (1998). Of interest is that *the differences in central pressure and wind speed do not become significant until the surface wind speed exceeds 65 m s^{-1}*, a value again close to that in Bister and Emanuel (1998). Because the present storm does not reach a steady state during the integration period, it remains unclear if the 65 m s^{-1} threshold is valid for other hurricane cases. Thus, more case studies need to be examined to determine if such a threshold would exist. Nevertheless, dissipative heating appears to be a more important process in intense hurricanes, such as Andrew, than weak ones. Its impact is negligible after landfall, for example, 68 h into the simulation in the present case, due to the rapid weakening of surface winds.

Figure 2 compares the horizontal distribution of the surface winds at 60 h into the simulations between the two runs. This time was chosen because the simulated storm is close to its deepest stage (see Fig. 1), and its western periphery is still several hundred kilometers away from the Florida coast. This time was also chosen for showing the horizontal distributions of other quantities that follow. The main feature of interest is the slightly smaller radius of maximum wind (RMW) in experiment DIS, with more axisymmetric distribution of wind speeds at the RMW; they are 5–8 m s^{-1} stronger than those in experiment CTL. This result is consistent with the observation that stronger hurricanes tend to be more compact (Willoughby et al. 1982). Outside the radius of 50 m s^{-1} winds, there are only minor differences between the two simulations.

Now let us examine the magnitude of dissipative heating rates compared to sensible heating rates (i.e., the vertical gradient of sensible heat flux). Figure 3 shows that the magnitudes of surface-layer dissipative heating rates (H_{DIS}) in experiment DIS are, on average, about twice as much as the sensible heating rates (H_{SEN}) in experiment CTL. Both increase with time until landfall of the storm. Of interest is that *the sensible heating rates in experiment DIS are negative, and opposite in sign and trend to those in experiment CTL,* a result that will be readily seen later (Fig. 5). The negative sensible heating rates offset partially the large positive dissipative heating, but the net (H_{NET}, sensible plus dissipative) surface-layer heating rates in experiment DIS are still

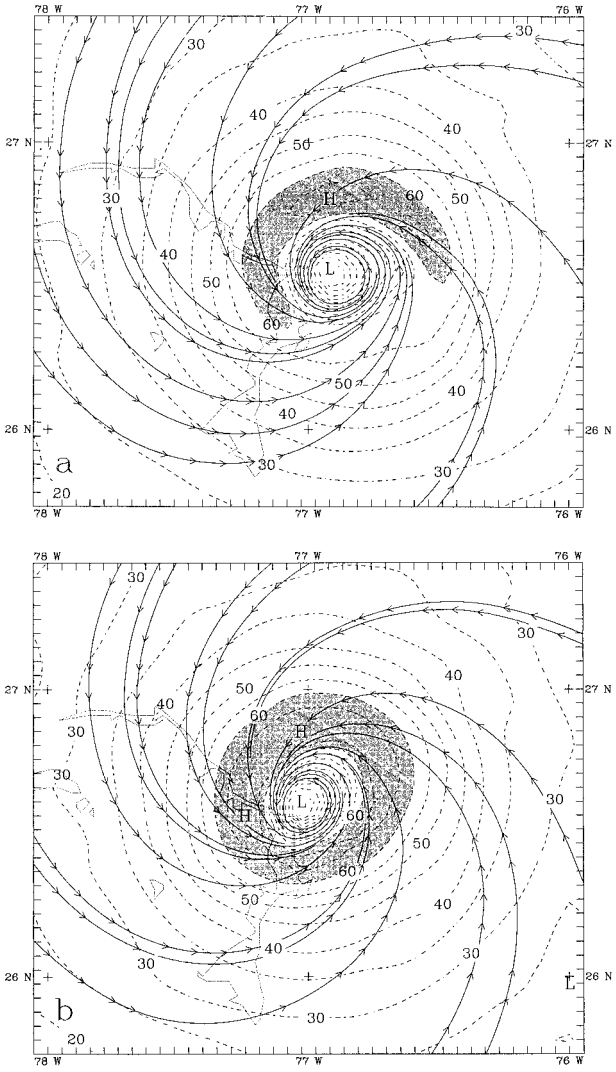

FIG. 2. Distribution of the surface layer streamlines (solid) and isotachs (dashed) at intervals of 5 m s^{-1} for a subdomain of the 6-km fine mesh at 60 h into the simulations from expts (a) CTL and (b) DIS. Wind speeds greater than 60 m s^{-1} are shaded. Tick marks along the perimeter are spaced at 6-km intervals.

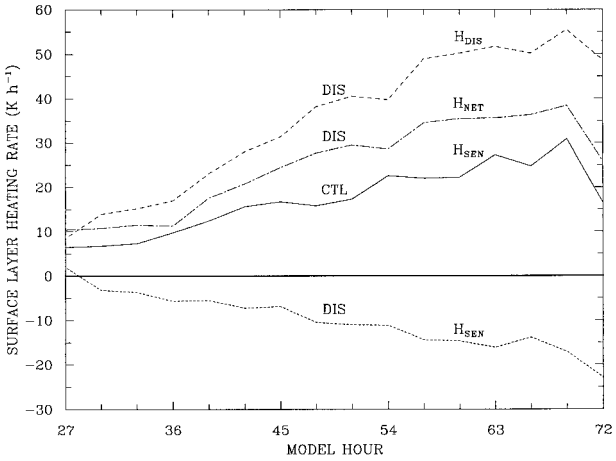

FIG. 3. Time series (3 hourly) of the averaged surface-layer heating rates (°C h^{-1}) associated with the vertical divergence of sensible heat flux (H_{SEN}) in expts CTL (solid) and DIS (dotted), and with the vertical divergence of dissipative heat flux (H_{DIS}, dashed) and net heat flux ($H_{NET} = H_{SEN} + H_{DIS}$, dot–dashed) in expt DIS. They are calculated by averaging over four points at the RMW located due north, east, south, and west of the storm center.

30%–40% greater than the sensible heating rates in experiment CTL. *It is this net increase of surface-layer heating that accounts for a more rapid deepening of the storm in experiment DIS.*

The horizontal distributions of the various surface layer heating rates are given in Fig. 4, which shows strong resemblance to the simulated surface wind field. For example, the sensible heating rates in experiment CTL are maximized at the RMW, as expected, with the largest value located in the northwestern quadrant. The rates are small (i.e., less than 5°C h^{-1}) outside the radius of 45 m s^{-1} winds (Fig. 4a). In contrast, the sensible heating rates in experiment DIS are negative everywhere except within the eye, and they are large negative at the RMW (Fig. 4b). Again, the rates are small beyond the radius of 45 m s^{-1} winds. The pattern of dissipative heating rates is closely correlated with that of the surface wind speed (Fig. 4c). It is of interest that although the overall effect of dissipative heating on the storm intensity is small for maximum winds <65 m s^{-1}, the instantaneous values of dissipative heating rates only become less than 5°C h^{-1} beyond the radius of 35 m s^{-1} winds. This indicates that *for winds <65 m s^{-1} the effect of dissipative heating on hurricane intensity may depend on the duration of model integration or storm structures.* The net heating rates for experiment DIS are also maximized at the RMW, and become small beyond the radius of 40 m s^{-1} winds (Fig. 4d), a value close to that in experiment CTL. Note that both the magnitude and radial gradient of the net heating rates are much greater than those in the control run.

The opposite trend in the surface sensible heating rates between experiments CTL and DIS can be seen from Fig. 5, which shows the time evolution of the averaged sensible heat fluxes at the RMW at the sea surface and at the top of the surface layer. The upward sea surface sensible fluxes in both runs (i.e., DIS_G and CTL_G) increase almost linearly with time, in agreement with the rapid increase of the surface winds at the RMW (cf. Figs. 5 and 1). However, the sea surface sensible heat flux (DIS_G) in experiment DIS is on average 100–150 W m^{-2} smaller than that (CTL_G) in experiment CTL after the surface winds exceed 55 m s^{-1}. Of particular significance is that the outgoing sensible flux at the top of the surface layer (DIS_T) in experiment DIS, which increases at a rate similar to the sea surface flux, is much *greater* than the incoming sea surface flux, whereas in experiment CTL the outgoing flux (CTL_T) remains nearly constant in time and is much *smaller* than the incoming sensible flux. This leads to the vertical flux di-

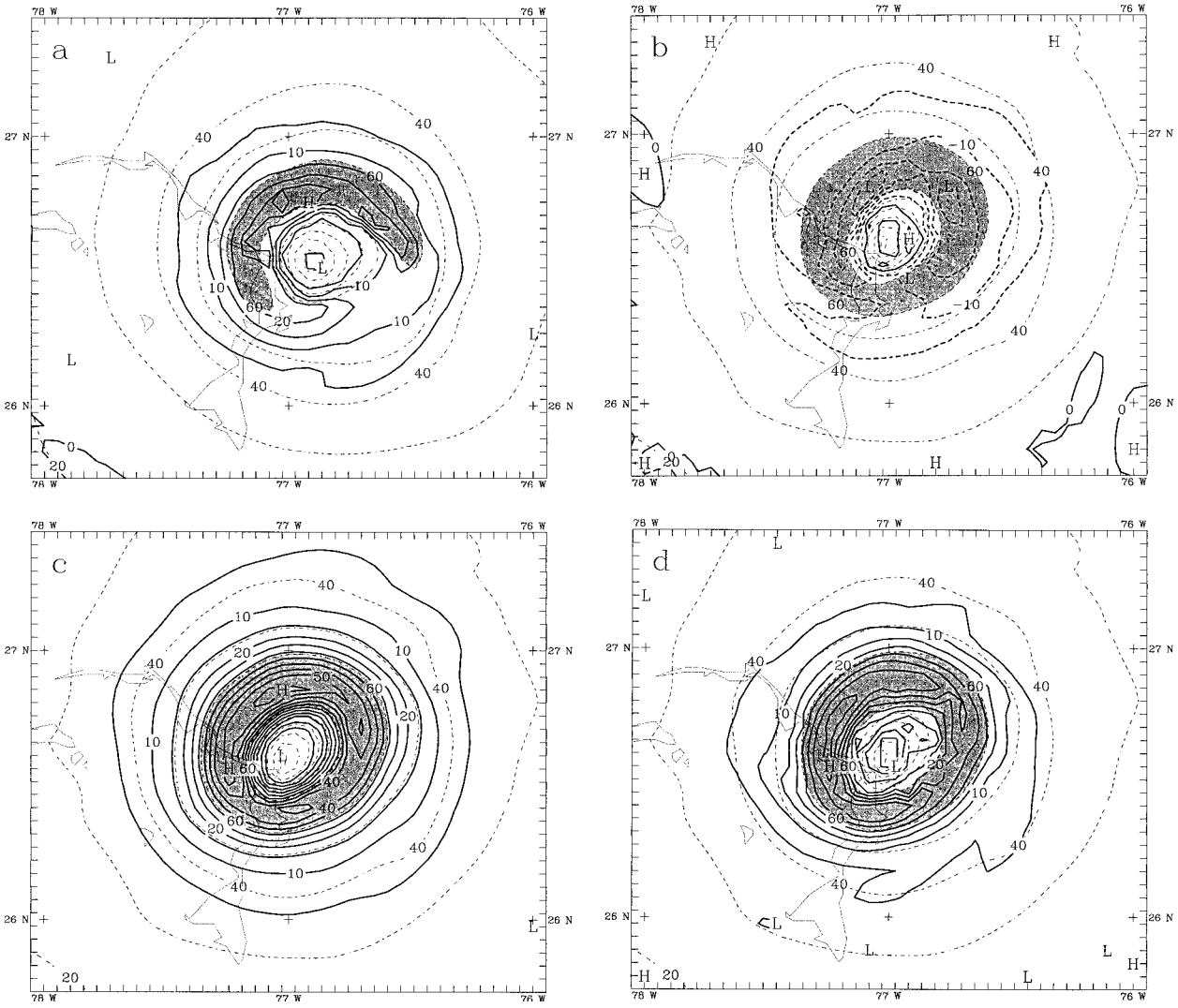

FIG. 4. As in Fig. 2 but for surface-layer heating rates, at intervals of 5°C h^{-1}, associated with the vertical divergence of sensible heat flux (H_{SEN}) in expts (a) CTL and (b) DIS; (c) the vertical divergence of dissipative heat flux (H_{DIS}), and (d) of net heat flux ($H_{NET} = H_{SEN} + H_{DIS}$) in expt DIS. Superposed are isotachs (thin dashed) at intervals of 10 m s^{-1}, with wind speeds greater than 40 m s^{-1} shaded. Solid (thick dashed) lines are positive (negative) values.

vergence (convergence) of sensible heating in experiment DIS (CTL), which acts to cool (warm) the surface layer (cf. Figs. 3 and 5).

The incorporation of dissipative heating accounts not only for the increased outgoing and the reduced incoming sensible fluxes, but also for the stability of the lowest layer. Figure 6 shows that the added dissipative heating in the surface layer reduces the potential temperature θ gradient below (the lowest half-σ level) and increases it above. For instance, the positive sea–air θ difference, maximized at the RMW, is always (0.5°–0.7°C) larger in experiment CTL than in experiment DIS (Fig. 6a). The differences between the two runs are negligible beyond the radius of 35 m s^{-1} winds where the sea–air θ difference in both runs becomes less than 2°C (not shown). This is responsible for the generation of weaker sea surface sensible fluxes in experiment DIS despite the presence of higher wind speeds than those in experiment CTL. On the other hand, the dissipative heating increases the virtual potential temperature θ_v difference between the surface level and that immediately above it (Fig. 6b), thereby leading to the increased outgoing sensible flux at the top of the surface layer. Although the θ_v difference in experiment DIS is three times as much as that in experiment CTL, it accounts for the nearly fourfold increase in sensible heat flux at the top of the surface layer (cf. Figs. 5 and 6b). It follows that *the dissipative heating tends to warm the surface layer, reducing the amount of upward sensible heat fluxes from the sea surface and statically destabilizing the boundary layers above.*

Finally, it should be mentioned that adding the dis-

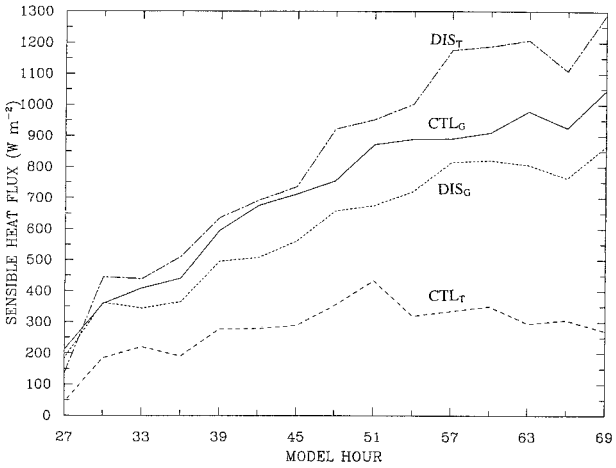

FIG. 5. As in Fig. 3 but for the averaged sensible heat flux (W m^{-2}), defined as $F = \rho c_{pm}\overline{w'T}$, at the sea surface (DIS$_G$ and CTL$_G$) and the top of the surface layer (DIS$_T$ and CTL$_T$) in expts CTL and DIS.

sipative heating produces very small differences in sea surface latent heat fluxes, so they are not shown. The averaged surface latent heat fluxes at the RMW increase from 900 W m^{-2} at 27 h to 2200 W m^{-2} at 60 h into the simulation, which are more than twice as great as the sensible heat fluxes. Both the simulated surface sensible and latent heat fluxes are comparable in magnitude to those estimated by previous observational investigators (see a summary given by Black and Holland 1995).

5. Summary and discussions

In this note, the effects of dissipative heating on hurricane intensity have been formulated and examined using a 72-h explicit simulation of Hurricane Andrew (1992) with a state-of-the-art, three-dimensional mesoscale model (i.e., MM5). The results have been discussed in light of the work of Bister and Emanuel (1998). Our results confirm their conclusion that the inclusion of dissipative heating results in a more intense hurricane. In the present case, dissipative heating accounts for an increase of central pressure by 5–7 hPa and maximum surface winds by 10% at the most intense stage when surface winds exceed 70 m s^{-1}. In the present case, however, the effect of dissipative heating does not appear to be significant until the surface wind exceeds 65 m s^{-1}. Whether or not 65 m s^{-1} is a threshold to indicate the significance of dissipative heating needs to be tested with more hurricane cases, since this value may depend on the duration of model integration, storm structures, and developing stages.

It is shown that the surface-layer heating rates and the sensible heat fluxes from the sea surface and the top of the surface layer are strongly affected by dissipative heating. In particular, the warming of the surface layer by dissipative heating results in a decrease in the surface

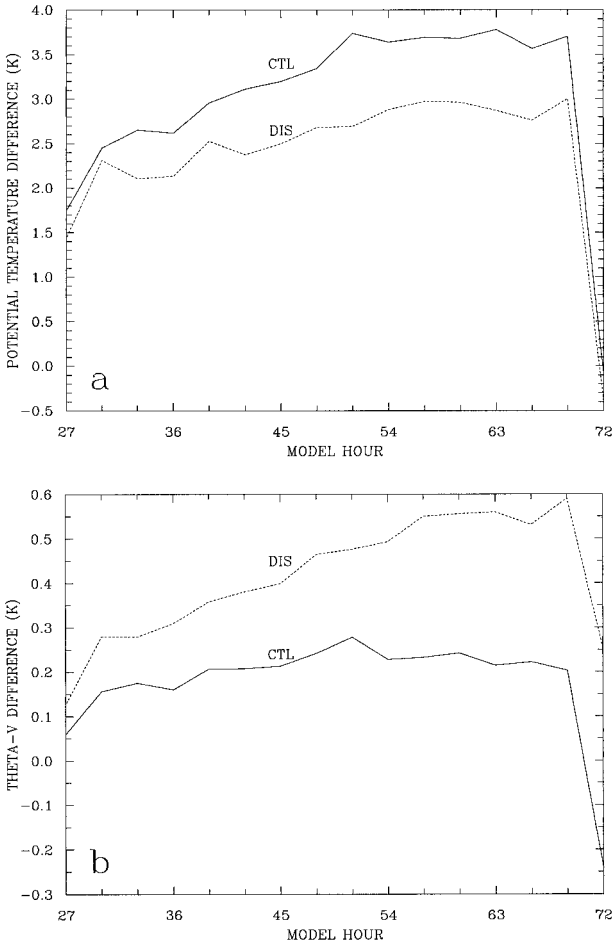

FIG. 6. As in Fig. 3 but for (a) the averaged potential temperature θ difference (°C) between the sea surface and the surface layer with a height interval of 40 m, and (b) the averaged virtual potential temperature θ_v difference (°C) between the surface layer and the overlying layer with a height interval of about 100 m, from expts CTL (solid) and DIS (dotted).

sensible flux and a large increase in the outgoing sensible flux at the top of the surface layer, leading to a net sensible heat flux divergence acting to cool the surface layer. The negative cooling rates partially counteract the dissipative heating rates, but the net (sensible plus dissipative) surface layer heating rates are still as much as 30%–40% greater than the sensible heating rates in the control simulation.

The questions of energy transfer into the ocean by the surface winds, feedback between SST and the wind-driven oceanic mixed layer, and heat transfer associated with evaporation of sea spray have been neglected in this study. Specifically, previous observational and numerical studies have shown that hurricanes can produce surface waves with heights in excess of 20 m, which in turn force the development of a surface mixed layer with an SST decrease by 3°–5°C within the inner core (Bender et al. 1993; Chang and Anthes 1978, 1979; Monaldo et al. 1997). This decrease in SST would coun-

teract the intensifying effect of dissipative heating, leading to the weakening of the storms. In contrast, the effect of sea spray evaporation on hurricane intensity is not straightforward. On the one hand, sea spray evaporation can produce a pronounced cooling in the surface layer when winds exceed 20 m s^{-1}, as reported by Fairall et al. (1994), which counteracts the dissipative heating effect. On the other hand, this evaporation will increase the surface-layer moisture content under the constraint of enthalpy conservation. This moisture would be eventually transported into the eyewall for latent heat release, providing a positive impact on the hurricane development. Moreover, the surface warming by dissipative heating may enhance the evaporation of sea spray, complicating further its impact on hurricane intensity. Thus, a coupled atmosphere–ocean model, in which dissipative heating and evaporation of sea spray are included, would be required to gain a more complete understanding of the combined effects of SST–intensity feedback, sea spray evaporation, and dissipative heating on the intensity of hurricanes.

Acknowledgments. We are grateful to Kerry Emanuel and two anonymous reviewers for their critical comments that helped improve the presentation of this manuscript. We are also grateful to Bob Adler for his generous support, Jim Carton for his discussion on the atmosphere–ocean interaction, and Yubao Liu and Wei Wang for their assistance in setting up the MM5 system on our DEC Alpha workstation. This work was supported by NSF Grant ATM-9802391 and NASA Grant NAG-57842. The second author (EA) was also supported by ATM-9502817 and NASA's GSRP program.

REFERENCES

Bender, M. A., I. Ginis, and Y. Kurihara, 1993: Numerical simulations of tropical cyclone–ocean interaction with a high-resolution coupled model. *J. Geophys. Res.,* **98,** 23 245–23 263.

Betts, A. K., and M. J. Miller, 1986: A new convective adjustment scheme. Part II: Single-column tests using GATE wave, BOMEX, ATEX and Arctic air-mass data sets. *Quart. J. Roy. Meteor. Soc.,* **112,** 693–709.

Bister, M., and K. A. Emanuel, 1998: Dissipative heating and hurricane intensity. *Meteor. Atmos. Phys.,* **55,** 233–240.

Black, P. G., and G. J. Holland, 1995: The boundary layer of Tropical Cyclone Kerry (1979). *Mon. Wea. Rev.,* **123,** 2007–2028.

Blackadar, A. K., 1979: High resolution models of the planetary boundary layer. *Advances in Environmental Science and Engineering,* J. Pfafflin and E. Ziegler, Eds., Vol. 1, Gordon and Breach Science Publishers, 50–85.

Chang, S. W., and R. A. Anthes, 1978: Numerical simulations of the ocean's nonlinear baroclinic response to translating hurricanes. *J. Phys. Oceanogr.,* **8,** 468–480.

——, and ——, 1979: The mutual response of the tropical cyclone and the ocean. *J. Phys. Oceanogr.,* **9,** 128–135.

Delsol, F., K. Miyakoda, and R. H. Clarke, 1971: Parameterized processes in the surface boundary layer of an atmospheric circulation model. *Quart. J. Roy. Meteor. Soc.,* **97,** 181–208.

Dudhia, J., 1989: Numerical study of convection observed during the winter monsoon experiment using a mesoscale two-dimensional model. *J. Atmos. Sci.,* **46,** 3077–3107.

——, 1993: A nonhydrostatic version of the Penn State–NCAR mesoscale model: Validation tests and simulation of an Atlantic cyclone and cold front. *Mon. Wea. Rev.,* **121,** 1493–1513.

Emanuel, K. A., 1995: The behavior of a simple hurricane model using a convective scheme based on subcloud-layer entropy equilibrium. *J. Atmos. Sci.,* **52,** 3960–3968.

Fairall, C. W., J. D. Kepert, and G. J. Holland, 1994: The effect of sea spray on surface energy transports over the ocean. *Global Atmos. Ocean Syst.,* **2,** 121–142.

Grell, G. A., J. Dudhia, and D. R. Stauffer, 1995: A description of the fifth generation Penn State/NCAR mesoscale model (MM5). NCAR Tech. Note 398+STR, 138 pp. [Available from NCAR Publications Office, P.O. Box 3000, Boulder, CO 80307-3000.]

Hellerman, S., and M. Rosenstein, 1983: Normal monthly wind stress over the world ocean with error estimates. *J. Phys. Oceanogr.,* **13,** 1093–1104.

Kurihara, Y., M. A. Bender, and R. Ross, 1993: An initialization scheme of hurricane models by vortex specification. *Mon. Wea. Rev.,* **121,** 2030–2045.

——, ——, R. E. Tuleya, and R. Ross, 1995: Improvements in the GFDL hurricane prediction system. *Mon. Wea. Rev.,* **123,** 2791–2801.

Liu, Y., D.-L. Zhang, and M. K. Yau, 1997: A multiscale numerical study of Hurricane Andrew (1992). Part I: Explicit simulation and verification. *Mon. Wea. Rev.,* **125,** 3073–3093.

Monaldo, F. M., T. D. Sikora, S. M. Babin, and R. E. Sterner, 1997: Satellite imagery of sea surface temperature cooling in the wake of Hurricane Edouard (1996). *Mon. Wea. Rev.,* **125,** 2716–2721.

Richman, J., and C. Garrett, 1977: The transfer of energy and momentum by the wind to the surface mixed layer. *J. Phys. Oceanogr.,* **7,** 876–881.

Rotunno, R., and K. A. Emanuel, 1987: An air–sea interaction theory for tropical cyclones. Part II: Evolutionary study using a nonhydrostatic axisymmetric numerical model. *J. Atmos. Sci.,* **44,** 542–561.

Stull, R. B., 1988: *An Introduction to Boundary Layer Meteorology.* Kluwer Academic, 666 pp.

Tao, W.-K., and J. Simpson, 1993: The Goddard cumulus ensemble model. Part I: Model description. *Terr. Atmos. Oceanic Sci.,* **4,** 35–72.

Willoughby, H. E., J. A. Clos, and M. G. Shoreibah, 1982: Concentric eyewalls, secondary wind maxima, and the evolution of the hurricane vortex. *J. Atmos. Sci.,* **39,** 395–411.

Zhang, D.-L., and R. A. Anthes, 1982: A high-resolution model of the planetary boundary layer—Sensitivity tests and comparisons with SESAME-79 data. *J. Appl. Meteor.,* **21,** 1594–1609.

——, E.-Y. Hsie, and M. W. Moncrieff, 1988: A comparison of explicit and implicit predictions of convective and stratiform precipitating weather systems with a meso-β scale numerical model. *Quart. J. Roy. Meteor. Soc.,* **114,** 31–60.